energies

MDPI

Article

Method for Evaluation of the Utility's and Consumers' Contribution to the Current and Voltage Distortions at the PCC

Yaroslav Shklyarskiy [1], Iuliia Dobush [1,*], Miguel Jiménez Carrizosa [2], Vasiliy Dobush [1] and Aleksandr Skamyin [3]

[1] Department of General Electrical Engineering, Saint Petersburg Mining University, 199106 Saint Petersburg, Russia; Shklyarskiy_YaE@pers.spmi.ru (Y.S.); dobush_vs@spmi.ru (V.D.)
[2] Departamento de Ingeniería Eléctrica, Universidad Politécnica de Madrid, E-28040 Madrid, Spain; miguel.jimenezcarrizosa@upm.es
[3] Department of Electric Power and Electromechanics, Saint Petersburg Mining University, 199106 Saint Petersburg, Russia; skamin_AN@pers.spmi.ru
* Correspondence: s185035@stud.spmi.ru

Abstract: In this article, a method that allows sharing responsibilities for the generation of harmonic currents between the utility and consumers powered by one point of common coupling (PCC) is addressed. For these purposes, mathematical modeling of the power supply system (PSS) with two consumers is carried out in order to introduce new indices using the simplest PSS structure as an example. Two indices are introduced that quantify the consumers' contribution to the distortion of current and voltage at the PCC and that evaluate harmonic emission from the utility side. Experimental tests are carried out where both linear and nonlinear loads are considered, capacitive loads are taken into account, and harmonic distortions from the utility side are modeled to show the applicability of the indices in a wide range of load types. The experiments confirmed the theoretical results and illustrated that the quantitative assessment of the contributions is unambiguous. It suggests that the proposed criterion could be a reasonable basis for further tax policy on harmonic pollution for each consumer at the PCC and for the utility.

Keywords: harmonics; distortion; power supply system; nonlinear load; distortion source

Citation: Shklyarskiy, Y.; Dobush, I.; Carrizosa, M.J.; Dobush, V.; Skamyin, A. Method for Evaluation of the Utility's and Consumers' Contribution to the Current and Voltage Distortions at the PCC. *Energies* **2021**, *14*, 8416. https://doi.org/10.3390/en14248416

Academic Editor: Julio Barros

Received: 8 November 2021
Accepted: 11 December 2021
Published: 13 December 2021

1. Introduction

The uses of nonlinear loads are rapidly increased at the different types of industrial enterprises. For example, renewable energy sources must be provided with semiconductor devices [1,2] and the mining industry uses a lot of nonlinear loads [3]. For instance, frequency converters and rectifiers cause production with high energy efficiency. This could be due to the new structure of the rectifier [4], new electromechanical transmission [5], new harmonic compensating device, or a method to implement it that allows a reduction of active power losses in the distribution network [6,7]. Additionally, semiconductor devices can become a basis for some low-power supply systems [8].

Besides the obvious advantages of using these types of loads, there is a drawback, namely, the widespread nonlinear loads lead to deterioration in the quality of electrical energy [9–11]. At the same time, power quality indicators must comply with both international standards (IEEE 1159-2019, IEEE 519-2014, IEC 61000-3-6) and national standards, for instance, the norms established in the Russian Federation (GOST 32144-2013). While GOST 32144-2013 regulates only the voltage distortion level, standard IEEE 519-2014 limits both voltage and current emissions. Concerning IEC 61000-3-6, it is stated that harmonics emissions have to be evaluated by comparing harmonic voltage vectors before and after load connection to the PCC. It is reasonable when a new consumer is going to be connected, but it cannot be used for distortion monitoring during uninterrupted loads operations.

In this regard, the scientific community has been faced with a number of tasks, namely, the development of methods and devices for harmonics compensation, and the development of methods for assessing the impact of each nonlinear consumer on the quality of electricity at the PCC [12,13]. The first issue has been considered in detail in [14–20], and various configurations of active, passive, and hybrid harmonics filters have been proposed. However, the issue of assessing the contribution of consumers to the deterioration of the electric power quality has not been fully resolved and there is no criterion that could quantify the tax of harmonic pollution for each consumer.

Nowadays, there are a number of methods that allow the dominant nonlinear load to be determined, which makes a greater contribution to network distortion.

The principle of some of them is based on the calculation of any type of power flow. These methods include the active power flow method [21,22], reactive power method [23], inactive power method [24], and distortion power method [25]. The authors of the reactive power method argue that the power direction method cannot be used for harmonic source detection [26]. Additionally, none of these methods provide accurate information about the contribution of each harmonics source to total distortion but identify just the dominant source. In addition, when calculations according to the above methods were presented in [27], the validity of the methods was investigated. The methods based on reactive power and the voltage-current ratio showed a higher sensitivity to the errors in the input data while the method based on the direction of active power flow gave invalid statements.

In [28], the Harmonic Pollution Metering method is proposed, which gives an advantage in terms of the accuracy and unambiguity of the results compared to the above methods. However, data on the complex impedance of both the PSS and consumers are required, which complicates the calculation process and the possibility of application.

There are also some methods based on the analysis of the currents and voltages vectors at the PCC. For example, in [29], the sharing of responsibilities for the generation of harmonic currents between PSS and consumers is performed by projecting the normalized vectors of current and voltage at the PCC on their vector sum for each harmonic separately. The disadvantage of this method is the presence of an inductive load in the consumption side, which increases their contribution to the deterioration of the electric power quality at the PCC, which leads to a biased assessment of the consumers' contribution.

On the other hand, there are multi points methods [30]. However, it is necessary to perform synchronized high-precision measurements to draw any conclusions about the location of the harmonics sources in the power supply system, which is a complex technical task.

Numerous works have been written about the effectiveness of the mentioned methods for identifying harmonics sources and determining the contribution of each of them to total distortion. For example, in [31], the articles [21–23,29,32] are criticized, and in [33], the drawbacks of [28,30,34] are considered.

As a result, none of these methods are officially stated by any of the power quality regulation standards because none of them allow quantification of the consumers' and utility's contributions accurately and reasonably. So, it is necessary to develop a new method to obtain an unambiguous result as a percentage correlation.

To sum up, it is obvious that an accurate method for determining harmonics sources should be developed soon in order to meet the needs of the modern energy industry. This global issue can be divided into two problems. The first one is the separation of distortions caused by PSS from distortions generated by all consumers connected to the PCC. The second question is sharing the responsibility for harmonics generation between consumers connected to the same PCC when there are no distortions caused by PSS or they are minimal. In this article, both issues are discussed.

Firstly, a method for determining the contributions of consumers to voltage and current distortions at the PCC is described. It is developed to quantify the responsibilities between consumers powered by the same PCC for harmonic currents generation when

there are minor distortions caused by the PSS. For this purpose, in Section 2, a mathematical modeling of the PSS with two consumers is carried out in order to introduce a new index using the simplest PSS structure as an example. Further, all conclusions can be applied to the PSS with a large number of consumers.

Secondly, a method for evaluation of the utility side contribution to harmonic distortion is developed. In Section 2.2.3, a mathematical modeling of the PSS with two consumers and grid side distortions is carried out and the second index is proposed, which evaluates the utility's contribution to the distortion at the PCC using a harmonic filter.

The experimental verification is shown in Section 3, where different types of loads are studied to illustrate that based on the proposed method and indices, it is impossible to identify the linear load as a harmonic source even if it includes capacitance. Additionally, it shows that this method is appropriate for nonlinear loads with different current spectra.

Finally, the obtained results, discussion, and some suggestions for future research are presented in Section 4.

2. Theoretical Model

2.1. The Method Development

For clarification of the method's understanding, the simplest equivalent circuit of the PSS with two consumers is shown in Figure 1.

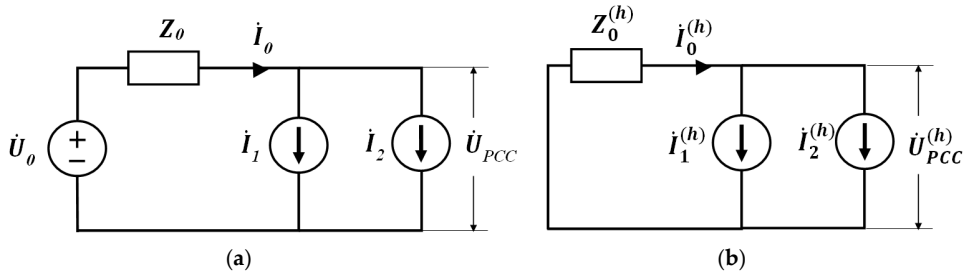

Figure 1. Equivalent circuit of PSS with two consumers: (**a**) general; (**b**) for harmonics.

In Figure 1, $\dot{U}_0$ is the PSS voltage source without harmonics, $\dot{U}_{PCC}$ is the voltage at the PCC, $\dot{I}_0$ is the PSS current, Z_0 is the PSS impedance, $\dot{I}_1$ /$\dot{I}_2$ are the first/second consumer's currents, $\dot{U}_{PCC}^{(h)}$ is the voltage at the PCC for harmonic number h, $Z_0^{(h)}$ is the PSS impedance for harmonic number h, and $\dot{I}_0^{(h)}$/ $\dot{I}_1^{(h)}$/ $\dot{I}_2^{(h)}$ are the harmonic current PSS/first/second consumer's.

Considering the superposition method, it is possible to consider two circuits: (a) at the first harmonic and (b) at the harmonics.

It can be seen that the non-sinusoidal network voltage $\dot{U}_{PCC}$ is proportional to the vector sum of the currents of the first and second consumers, when the PSS impedance Z_0 is constant according to Formula (1):

$$\dot{U}_{\mathrm{PCC}}^{(h)} = \dot{I}_0^{(h)} \cdot Z_0^{(h)} = \left(\dot{I}_1^{(h)} + \dot{I}_2^{(h)}\right) \cdot Z_0^{(h)} \quad (1)$$

In this way, two important conclusions should be highlighted. The first one is that proceeding from assessing the voltage quality to assessing the current quality is a possible and extremely important step, despite its the non-obviousness, since some national standards regulate only the total harmonic distortion of the voltage (*THDu*) but not the total harmonic distortion of the current (*THDi*). The second conclusion is that it is necessary to evaluate the contribution of each consumer to the total current and voltage distortion at the PCC in vector form.

Additionally, it should be noted that voltage distortions at the PCC depend on the value of PSS's complex impedance. Due to the fact that in real power systems, its value is never equal to zero, the current distortions always cause voltage distortions.

In this regard, the next step is to consider the different relative positions of the currents' vectors. All possible options were classified into four cases, presented in Figure 2. For each case, the PSS current's vector $\dot{I}_{0}^{(h)}$ is located horizontally, and they differ in the ratio of the projections of the consumer's current vectors $\dot{I}_{1}^{(h)}/\dot{I}_{2}^{(h)}$ on the total current vector $\dot{I}_{0}^{(h)}$, which are respectively equal to $\dot{I}_{1pr}^{(h)}$ and $\dot{I}_{2pr}^{(h)}$. Additionally, the vector diagrams show the angle α between the vectors $\dot{I}_{1}^{(h)}$ and $\dot{I}_{2}^{(h)}$, β between the vectors $\dot{I}_{1}^{(h)}$ and $\dot{I}_{0}^{(h)}$, and γ between the vectors $\dot{I}_{2}^{(h)}$ and $\dot{I}_{0}^{(h)}$.

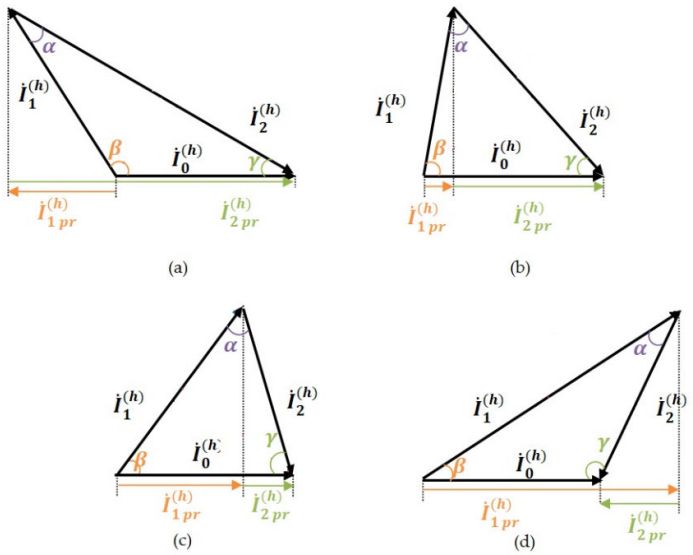

Figure 2. Relative positions of the currents' vectors: **(a)** $K_{D1}^{(h)} < 0\%$; **(b)** $K_{D1}^{(h)} > 0\%$ and the second consumer is a dominant source of distortions; **(c)** $K_{D1}^{(h)} > 0\%$ and the first consumer is a dominant source of distortions; **(d)** $K_{D1}^{(h)} > 100\%$.

In order to calculate the contribution of the first and second consumers to the current and voltage distortions at the PCC, the ratio of the projection of the consumer's harmonic current vector on the PSS harmonic current vector to the PSS harmonic current vector is proposed according to the following expressions:

$$K_{D1}^{(h)} = \frac{I_{1pr}^{(h)}}{I_{0}^{(h)}} \cdot 100\% \quad (2)$$

$$K_{D2}^{(h)} = \frac{I_{2pr}^{(h)}}{I_{0}^{(h)}} \cdot 100\% \quad (3)$$

For the case shown in Figure 2a, the contribution of the first consumer is $K_{D1}^{(h)} < 0\%$, since the vector $\dot{I}_{1pr}^{(h)}$ is opposite to $\dot{I}_{0}^{(h)}$. At the same time, $K_{D2}^{(h)} > 100\%$ indicates that the second consumer is the dominant source of distortions at the harmonic h, and the non-sinusoidal current of the first consumer compensates for the distortions generated by the second consumer. In contrast, in the case shown in Figure 2d, $K_{D1}^{(h)} > 100\%$, $K_{D2}^{(h)} < 0\%$, and consequently, the current of the second consumer compensates for the current of the first one. So, these relative positions of vectors indicate that one of the consumers is the harmonic source and another is the linear load.

The rest of the cases are intermediate options of the vectors' location, where the values of both contributions are in the interval (0; 100), which means both consumers are harmonic sources.

Analyzing these cases, it is clear that the larger the magnitude of the consumer current vector, the greater the contribution to the total current vector regardless of the vectors' relative position. Namely, in Figure 2, the dominant source of distortion is the first consumer in both top schemes, and it is the second consumer in both bottom schemes.

The following key findings can be drawn from the above mathematical calculations:

- The influence of each consumer is estimated by the value of the projection of the consumer current vector on the total current vector separately for each harmonic *h*;
- The greater the consumer's harmonic current's projection, the greater the contribution;
- To carry out calculations, it is necessary to know the magnitude and phases of harmonic currents.

2.2. Assessment of the Parameters That Influence on the Results of KD1(h) Calculation

The next step is to define the parameters that affect the results of the calculations according to the proposed method and assess this influence. The following parameters were chosen:

- Consumers with a mixed structure, namely, that include both linear and nonlinear loads;
- Consumers with capacitances, for instance, power factor correctors or harmonic filters;
- Additional grid side distortions.

Now, all of these parameters are considered in detail.

2.2.1. Mixed Structure Consumers

The previous scheme (Figure 1) does not take into account the influence of the harmonic currents of the first consumer on the consumed current of the second one and vice versa. Since real consumers cannot be divided exclusively into sources or consumers of harmonics, the following equivalent circuit (Figure 3) is considered. Electric power consumers are represented by both the current sources and the linear loads to show their generation and consumption of harmonic currents.

In Figure 3, $\dot{I}_{0}^{(h)}$ is the PSS harmonic current, $Z_{0}^{(h)}$is the PSS impedance for harmonic *h*, $\dot{I}_{1}^{(h)}/\dot{I}_{2}^{(h)}$ is the first/second consumer's harmonic current, $\dot{I}_{1nl}^{(h)}/\dot{I}_{2nl}^{(h)}$ is the non-sinusoidal current generated by the nonlinear load of the first/second consumer, and $\dot{I}_{1l}^{(h)}/\dot{I}_{2l}^{(h)}$ is the non-sinusoidal current consumed by the linear load of the first/second consumer.

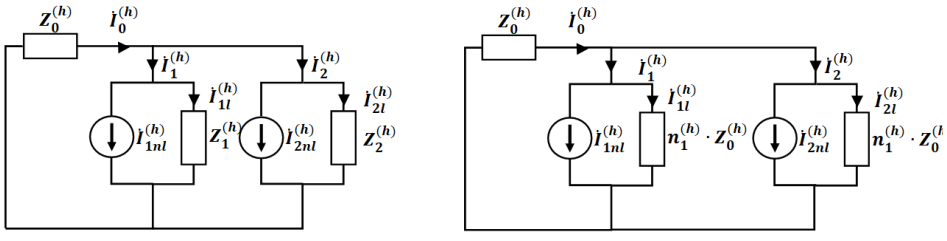

Figure 3. Equivalent circuit with mixed structure consumers: (**a**) for harmonic currents; (**b**) for harmonic currents with introduced coefficients.

To simplify the calculations, the coefficients $\dot{n}_{1}^{(h)}$ and $\dot{n}_{2}^{(h)}$ are introduced, showing how many times the consumers' impedances $Z_{1}^{(h)}$ and $Z_{2}^{(h)}$ are greater than the PSS impedance $Z_{0}^{(h)}$:

$$\dot{n}_1^{(h)} = \frac{Z_1^{(h)}}{Z_0^{(h)}} \tag{4}$$

$$\dot{n}_2^{(h)} = \frac{Z_2^{(h)}}{Z_0^{(h)}} \tag{5}$$

The proposed system is solved by the superposition method and the calculated currents are as follows:

$$\dot{I}_0^{(h)} = \frac{\dot{n}_1^{(h)} \cdot \dot{n}_2^{(h)}}{\dot{n}_1^{(h)} \cdot \dot{n}_2^{(h)} + \dot{n}_1^{(h)} + \dot{n}_2^{(h)}} \cdot \left(\dot{I}_{1nl}^{(h)} + \dot{I}_{2nl}^{(h)}\right) \tag{6}$$

$$\dot{I}_1^{(h)} = \frac{\dot{n}_1^{(h)} + \dot{n}_1^{(h)} \cdot \dot{n}_2^{(h)}}{\dot{n}_1^{(h)} \cdot \dot{n}_2^{(h)} + \dot{n}_1^{(h)} + \dot{n}_2^{(h)}} \cdot \dot{I}_{1nl}^{(h)} - \frac{\dot{n}_2^{(h)}}{\dot{n}_1^{(h)} \cdot \dot{n}_2^{(h)} + \dot{n}_1^{(h)} + \dot{n}_2^{(h)}} \cdot \dot{I}_{2nl}^{(h)} \tag{7}$$

$$\dot{I}_2^{(h)} = -\frac{\dot{n}_1^{(h)}}{\dot{n}_1^{(h)} \cdot \dot{n}_2^{(h)} + \dot{n}_1^{(h)} + \dot{n}_2^{(h)}} \cdot \dot{I}_{1nl}^{(h)} + \frac{\dot{n}_2^{(h)} + \dot{n}_1^{(h)} \cdot \dot{n}_2^{(h)}}{\dot{n}_1^{(h)} \cdot \dot{n}_2^{(h)} + \dot{n}_1^{(h)} + \dot{n}_2^{(h)}} \cdot \dot{I}_{2nl}^{(h)} \tag{8}$$

It can be seen that the currents of consumers $\dot{I}_{1}^{(h)}$, $\dot{I}_{2}^{(h)}$ consist of both the harmonic current generated by the consumer itself $\dot{I}_{1nl}^{(h)}$ and $\dot{I}_{2nl}^{(h)}$, respectively, where the proportionality factor is represented by Formula (9), and the harmonic current of another consumer $\dot{I}_{2nl}^{(h)}$ and $\dot{I}_{1nl}^{(h)}$:

$$\dot{C} = \frac{\dot{n}_1^{(h)} \cdot \dot{n}_2^{(h)}}{\dot{n}_1^{(h)} + \dot{n}_2^{(h)} + \dot{n}_1^{(h)} \cdot \dot{n}_2^{(h)}} \tag{9}$$

Harmonic currents caused by other consumers flow through the lines of consumers in proportion to the coefficients $\dot{A}$ and $\dot{B}$, which directly depend on the parameters of consumers relative to the PSS impedance:

$$\dot{A} = \frac{\dot{n}_1^{(h)}}{\dot{n}_1^{(h)} + \dot{n}_2^{(h)} + \dot{n}_1^{(h)} \cdot \dot{n}_2^{(h)}} \tag{10}$$

$$\dot{B} = \frac{\dot{n}_2^{(h)}}{\dot{n}_1^{(h)} + \dot{n}_2^{(h)} + \dot{n}_1^{(h)} \cdot \dot{n}_2^{(h)}} \tag{11}$$

Based on these expressions, the following conclusions can be drawn. The consumer's contribution $K_{D1}^{(h)}$ directly depends on $\dot{I}_1^{(h)}$. In turn, $\dot{I}_1^{(h)}$ depends on both $\dot{I}_{1nl}^{(h)}$ and $\dot{I}_{2nl}^{(h)}$, which means the second consumer affects $K_{D1}^{(h)}$. However, this influence can be evaluated by the coefficient $\dot{B}$, which is $\dot{n}_1^{(h)}$ times smaller than $\dot{C}$. Obviously, when a stiff utility system is considered with less than a 5% voltage drop across $Z_{0}^{(1)}$, the influence of the second consumer on the contribution $K_{D1}^{(h)}$ is negligible and decreases with the number of harmonics *h*. Similar reasoning can be provided for the influence of the first consumer on $K_{D2}^{(h)}$. Additionally, conclusions for systems with three or more consumers can be drawn in the same way.

Thus, for the considered conditions, the proposed method and index allow evaluation of the contributions of the consumers that include both linear and nonlinear loads.

2.2.2. Consumers with a Capacitance

This type of load should be considered separately, since its frequency properties differ from the inductance and resistance. The most common types of capacitive loads are power factor correctors and harmonic filters. In Figure 4, equivalent circuits with a nonlinear load and resistive and inductive linear load and capacitive load are shown.

A harmonic filter is presented as capacitance $c_{HF}^{(h)}$ and inductance $L_{HF}^{(h)}$, which, when connected in series, create a resonant circuit with a nonlinear load for harmonic *h*. In this regard, most of the current generated by the nonlinear load flows through the filter, which is the essence of using the filter as shown in Figure 4a. So, there is no sense to calculate the projection of $\dot{I}_{nl}^{(h)}$, $\dot{I}_{l}^{(h)}$, and $\dot{I}_{\mathrm{HF}}^{(h)}$ on $\dot{I}_{0}^{(h)}$ because $\dot{I}_{0}^{(h)}$ tends to zero and $K_D^{(h)}$ tends to infinity. Basically, the harmonic emission problem for harmonic *h* is solved in this situation. Concerning other harmonics, the impedance of the harmonic filter increases according to the increase in the impedance of $L_{HF}^{(h)}$. So, the harmonic filter for the non-resonant frequency shows the properties of the linear load, which is confirmed further in Section 3.2.2.

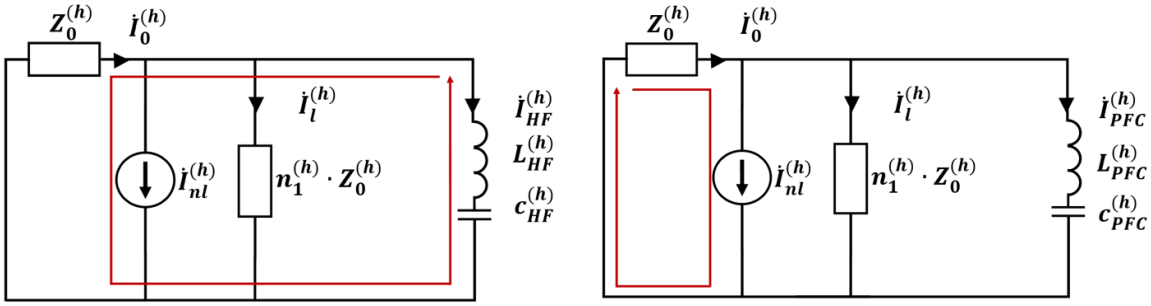

Figure 4. Equivalent circuit with capacitance: (**a**) with a harmonic filter; (**b**) with a power factor corrector.

Considering the power factor correctors, most of them include the inductance $L_{PFC}^{(h)}$, which, firstly, decreases the starting current and, secondly, creates a resonant circuit for the frequency that is lower than the smallest harmonic. Since it is the 3rd harmonic, the resonant frequency is, for example, 134 Hz. It leads us to the conclusion that, similarly to the harmonic filters, power factor correctors have the properties of linear loads for non-resonant frequencies. It means the currents $\dot{I}_{PFC}^{(h)}$ and $\dot{I}_{l}^{(h)}$ are of the same order of magnitude. A detailed analysis of the contribution of the power factor corrector with a detuned frequency of 134 Hz is presented in Section 3.2.2.

2.2.3. Additional Grid Side Distortions

Except distortions generated by the consumers, it is possible that the PCC is powered by the non-sinusoidal voltage $\dot{U}_{PSS}^{(h)}$ as shown in Figure 5. Then, all loads connected to the PCC pass current are caused by grid side distortions.

Considering Figure 5a, the nonlinear load is the least affected by non-sinusoidal voltage because it can be replaced by $\dot{I}_{l}^{(h)}$, which remains constant regardless of the grid parameters. This feature is typical for most types of nonlinear loads, and for this reason, replacement with current sources is a common practice. However, not all nonlinear loads are independent of the external conditions, so the question of nonlinear loads' equivalent circuits is a topic for additional research. Concerning linear loads and power factor correctors, the non-sinusoidal voltage $\dot{U}_{PSS}^{(h)}$ causes currents that are drawn as red and green lines in Figure 5a, respectively. If the grid side distortion is not significant compared to the nonlinear load, then these currents are much less than $\dot{I}_{nl}^{(h)}$ and do not affect $K_D^{(h)}$. This situation is considered in Section 3.2.4. If the dominant harmonic source is located at the utility side, then these currents increase considerably and $K_D^{(h)}$ does not represent accurate information. However, in this case, identification of the grid side harmonic source is essential to transfer the obligation to compensate for these distortions from the consumer to the PSS.

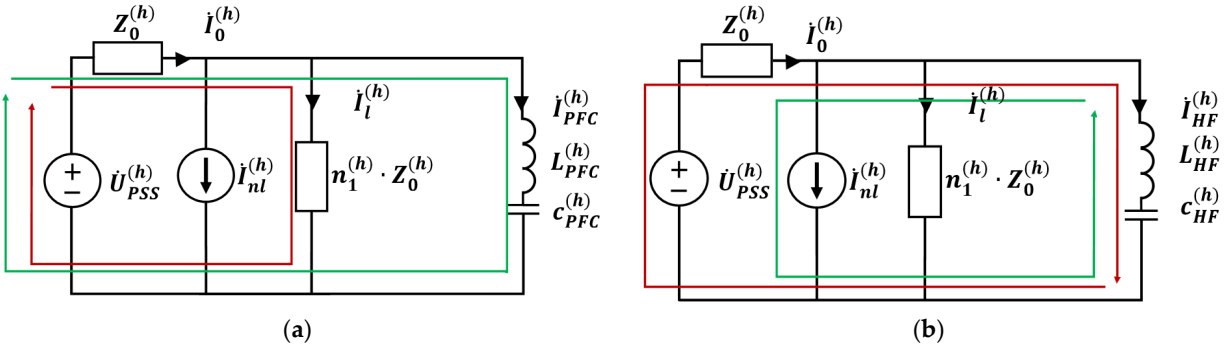

Figure 5. Equivalent circuit with grid side distortions and: (**a**) with a power factor corrector; (**b**) with a harmonic filter.

To solve this problem, the harmonic filter can be used as suggested in [35]. It is shown in Figure 5b that when the harmonic filter is connected at the PCC, then the non-sinusoidal current generated by the nonlinear load flows mainly through the filter (green line). At the same time, the non-sinusoidal current caused by $\dot{U}_{PSS}^{(h)}$ also flows through the resonant circuit. It means that the new index can be introduced to calculate the contributions of the PSS and the consumers' contribution according to the following equations:

$$K_{D\,PSS/HF}^{(h)} = \frac{I_0^{(h)} \cdot cos\left(\psi_{I0}^{(h)} - \psi_{IHF}^{(h)}\right)}{I_{HF}^{(h)}} \cdot 100\% \quad (12)$$

$$K_{D\,nl/HF}^{(h)} = \frac{-I_{nl}^{(h)} \cdot cos\left(\psi_{Inl}^{(h)} - \psi_{IHF}^{(h)}\right)}{I_{HF}^{(h)}} \cdot 100\% \quad (13)$$

where $\psi_{I0}^{(h)}$ is the phase of $\dot{I}_0^{(h)}$, $\psi_{IHF}^{(h)}$ is the phase of $\dot{I}_{HF}^{(h)}$, and $\psi_{Inl}^{(h)}$ is the phase of $\dot{I}_{nl}^{(h)}$. When the dominant source at the grid side is detected, further calculation of the consumer contributions is not rational since the problem must be solved outside the investigated section of the power system. When there is a dominant source at the consumer's side, the contributions can be calculated according to Formulas (2) and (3). This example is considered in Section 3.2.4.

2.3. The Method's Algorithm

Based on the information above, the algorithm of the proposed method was completed (Figure 6).

1. Identification of the utility contribution to the distortion of the current and voltage at the PCC:
   - Separately, for each harmonic, the amplitudes and phases of the PSS's harmonic currents $\dot{I}_{0^{(h)}}$ and the harmonic filter currents $\dot{I}_{HF}^{(h)}$ are measured for the resonant frequency *h*. The previously installed filter can be used or an additional filter should be connected as part of the measuring equipment. All required data can be obtained by a standard power quality analyzer;
   - Calculations of the PSS contribution are made according to (12). If the utility is the dominant source (contribution is more than 50%), then no additional measures to eliminate harmonics at the consumer's side should be provided since the measures from the utility side are paramount. If the grid side distortions are low, then sharing of the responsibilities for harmonic generation between consumers can be achieved.
2. Sharing responsibilities for harmonic generation between consumers:
   - Separately, for each harmonic, the amplitudes and phases of the PSS's currents $\dot{I}_{0^{(h)}}$ and all consumers' currents $\dot{I}_1^{(h)}$, $\dot{I}_2^{(h)}$, …, $\dot{I}_n^{(h)}$ are measured;

- Calculation of each consumers' contribution using the following equation is done (14):

$$K_{Dj}^{(h)} = \frac{I_{\mathrm{j}}^{(h)} cos\left(\psi_{Ij}^{(h)} - \psi_{I0}^{(h)}\right)}{I_0^{(h)}} \cdot 100\% \quad (14)$$

where $I_{\mathrm{j}}^{(h)}$is the *j*-th consumer's current of harmonic *h*, $\psi_{Ij}^{(h)}$ is the phase of $\dot{I}_j^{(h)}$, $I_0^{(h)}$ is the PSS current of harmonic *h*, and $\psi_{I0}^{(h)}$ is the phase of $\dot{I}_0^{(h)}$.

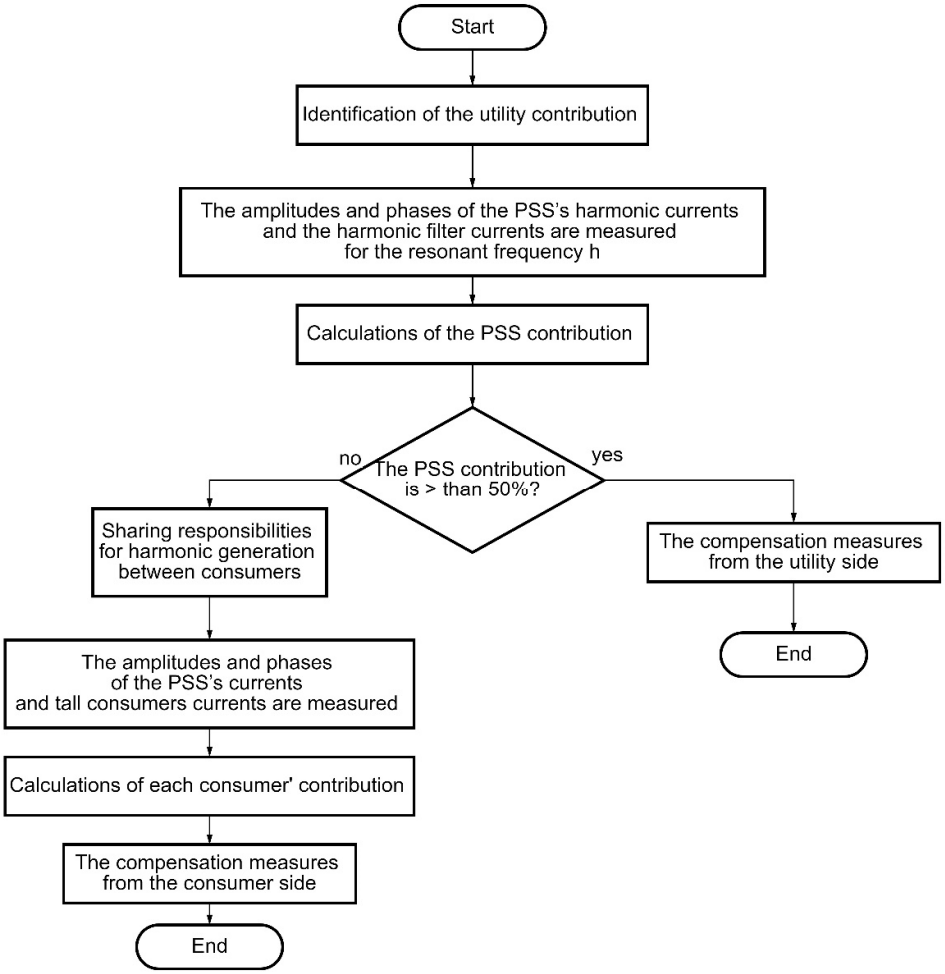

Figure 6. The method's algorithm.

Based on these values, some recommendations on harmonic compensation can be formulated. It is especially important for cases when the investigated part of the power system consists of several voltage levels and several busses where harmonic filters can be connected. Additionally, new methodology for additional charges (penalties) for harmonic emissions can be developed.

In the next Section 3, laboratory experiments are described that illustrate the particular cases mentioned above in order to show the applicability of the proposed method and to confirm the reasoning about different types of loads given above.

3. Laboratory Experiment

3.1. Laboratory Branch

To test the proposed method for determining the contribution of consumers to the deterioration of the voltage and current quality at the PCC K_D, an experimental test bench was developed as Figure 7 shows.

It consists of:

- A three-phase sinusoidal voltage source (line voltage is 380 V);
- Three coils L_S with variable inductance from 0.3 to 12 mH, connected in series with the network to create an additional voltage drop before the PCC;
- Three resistors R_s = 2.2 Ohm that can be connected to the PSS in series;
- A linear load as an AIR 90L6 induction motor (*M*) with a nameplate power of 1.5 kW, loaded by a P32M DC motor with a nameplate power of 1.1 kW, operating in the generator mode;
- A thyristor rectifier (*TR*) TVN-3-L-230-125, designed for an input line voltage of 380 V, an output voltage up to 230 V, and a rated current of 125 A. The *TR* is loaded with a 6-kW active resistance as the electric heating tubes (EHT_1);
- A three-phase thyristor power controller (*TPC*) TRM-3M-30, designed for an input line voltage of 380 V and maximum load current of 30 A. Similarly, the *TPC* is loaded by EHT_2 but with a lower power 1.5 kW;
- A 5th harmonic filter (*HF*);
- A power factor corrector (*PFC*) with a detuned frequency of 134 Hz, with four steps of regulation, which are 0.5 kvar, and one 1 kvar step of regulation.

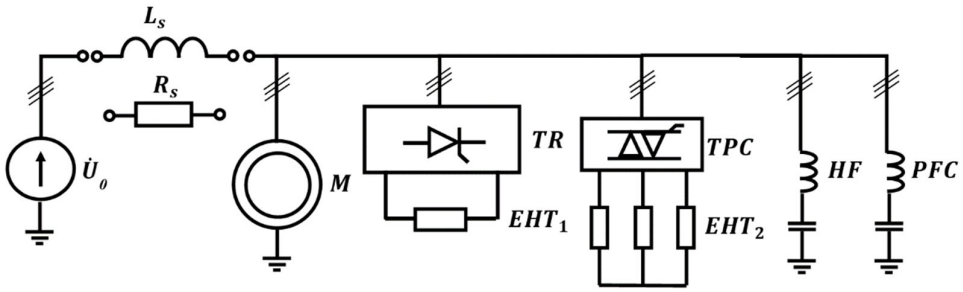

Figure 7. General laboratory branch scheme.

Measurements of the currents and voltages were carried out using the Fluke 125B power quality analyzer, which allows the amplitudes and phases of the measured values from the 1st to the 40th harmonics to be determined.

3.2. List of the Experiments

As part of the study, four blocks of experiments were carried out:

- Block 1. Experiments with no additional grid side distortions and without any capacitive loads;
- Block 2. Experiments with no additional grid side distortions and with two types of capacitive loads;
- Block 3. Experiments with additional grid side distortions and without any capacitive loads;
- Block 4. Experiments with additional grid side distortions and with two types of capacitive loads.

A detailed description of the experiments for each block is presented below.

3.2.1. Experiments of the Block 1

To conduct the experiments of block 1, a laboratory branch was assembled according to the scheme shown in Figure 8.

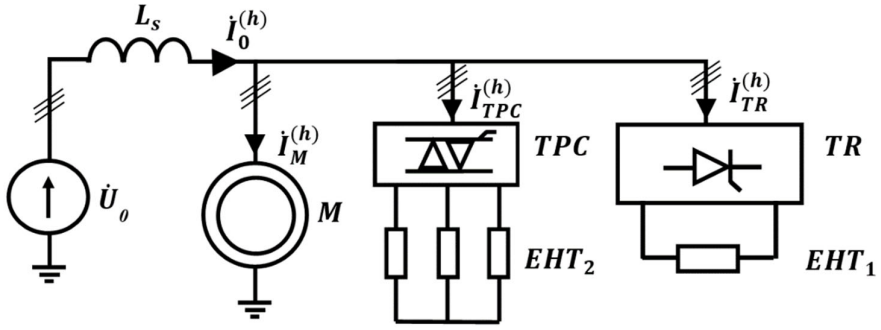

Figure 8. Laboratory branch scheme for block 1.

Based on the used equipment, the following experiments were conducted, the parameters of which are described in Table 1.

Table 1. The equipment parameters for the experiments of block 1.

	L_S, mH	*TR*, U_d%	*TPC* U_c%	*M*, kW
Experiment 1	0.1	15÷55	-	1.04
Experiment 2	0.1	40	-	0÷1.04
Experiment 3	0.1	-	10÷50	1.04
Experiment 4	0.1	-	40	0÷1.04

According to Experiment 1, the voltage of *TR's* DC-side was regulated as the value U_d as a percentage correlation. At the same time, the output voltage of *TPC* was varied as a percentage of the control voltage U_c for Experiment 3. Experiments 2 and 4 were conducted while *M's* load was changed from no-load mode to 1 kW. During each experiment, the harmonic currents $\dot{I}_{0^{(h)}}$, $\dot{I}_{TR^{(h)}}$/ $\dot{I}_{TPC^{(h)}}$, and $\dot{I}_{M^{(h)}}$ were measured and the contributions $K_{DTR}^{(h)}/K_{DTPC}^{(h)}$ and $K_{DM}^{(h)}$ were calculated.

The waveform of the currents measured during Experiments 1 and 2 are shown in Figure 9a. The calculation results for the fifth harmonic are presented in Figure 9b,c. The same data for Experiments 3 and 4 is shown in Figure 10.

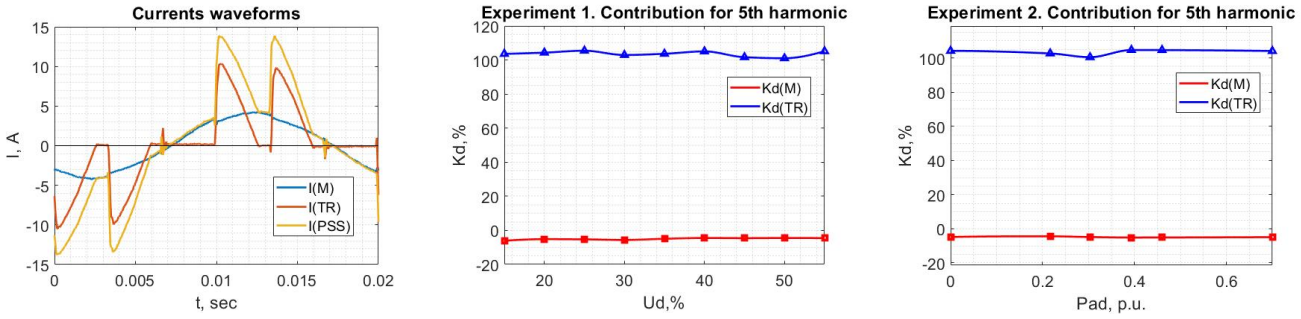

(**a**) (**b**) (**c**)

Figure 9. Results of Experiment 1 and Experiment 2 for the 5th harmonic: (**a**) waveform of the currents; (**b**) calculation results of Experiment 1; and (**c**) calculation results of Experiment 2.

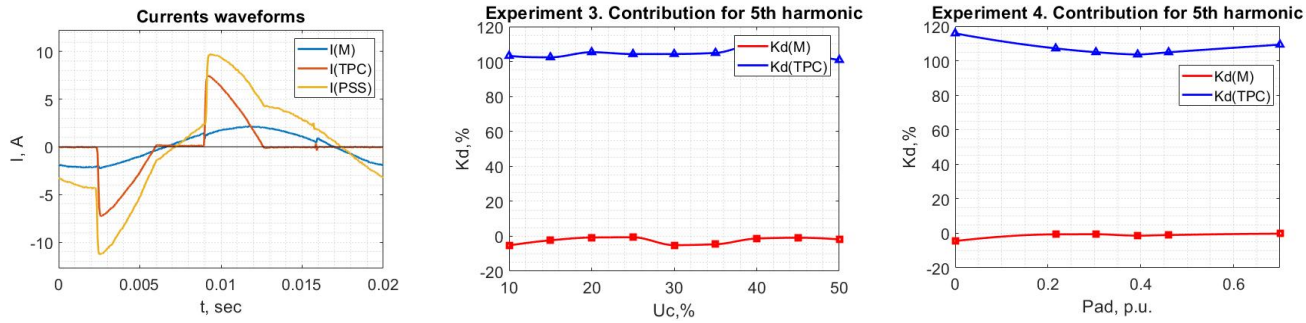

Figure 10. Results of Experiment 3 and Experiment 4 for the 5th harmonic: (**a**) waveform of currents; (**b**) calculation results of Experiment 3; (**c**) calculation results of Experiment 4.

Calculated by the proposed method, the consumer's contribution to the current and voltage distortion at the PCC for each harmonic has a negative value for *M*. It indicates that the harmonic current flowing through the motor compensates for the non-sinusoidal current caused by the presence of *TR* and *TPC* in the system, and the linear consumer itself is not a harmonic source. The proposed contribution $K_D^{(h)}$ is expressed as a stable value above 100% for the harmonic sources. Thus, it is emphasized that the calculated values of the contributions are equal under the various operating modes of linear and nonlinear loads.

3.2.2. Experiments of Block 2

The experiments of block 2 are different from block 1 due to the presence of capacitive loads, which are shown in Figure 11.

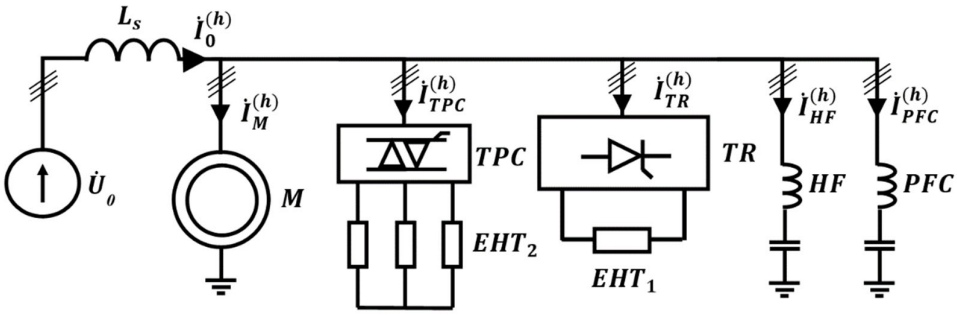

Figure 11. Laboratory branch scheme for block 2.

Experiments were carried out according to the parameters described in Table 2.

Table 2. The equipment parameters for the experiments of block 2.

	L_S, mH	*TR*, U_d%	*TPC* U_c%	*M*, kW	*HF*	*PFC's* Capacitance, kvar
Experiment 1	0.1	15÷55	-	1.04	+	-
Experiment 2	0.1	-	10÷50	1.04	+	-
Experiment 3	0.1	15÷55	-	-	-	2
Experiment 4	0.1	40	-	-	-	0–3

During each experiment, the harmonic currents $\dot{I}_{0^{(h)}}$, $\dot{I}_{TR^{(h)}}/\dot{I}_{TPC^{(h)}}$, $\dot{I}_{HF^{(h)}}/\dot{I}_{PFC^{(h)}}$, and $\dot{I}_{M^{(h)}}$ were measured and the contributions $K_{D\,TR}^{(h)}/K_{D\,TPC}^{(h)}$, $K_{D\,HF}^{(h)}/K_{D\,PFC}^{(h)}$, and $K_{DM}^{(h)}$ were calculated relative to $\dot{I}_{0^{(h)}}$. In addition, the contributions $K_{D\,TR/F}^{(h)}/K_{D\,TPC/F}^{(h)}$, $K_{D\,0/F}^{(h)}$, and $K_{DM/F}^{(h)}$ relative to $\dot{I}_{HF^{(h)}}$ were found for Experiments 1 and 2.

The waveforms of the currents measured during Experiment 1 are shown in Figure 12a. The calculation of the contributions for the fifth harmonic relative to the PSS is presented in Figure 12b. Additionally, the contributions relative to the filter are described in Figure 12c. Data on the non-resonant frequency for Experiment 1 is shown in Figure 13. The same data for resonant frequency of Experiment 2 is shown in Figure 14. Concerning Experiments 3 and 4, the currents' waveforms are shown in Figure 15a, while the contributions relative to the current of PSS are shown in Figure 15b,c.

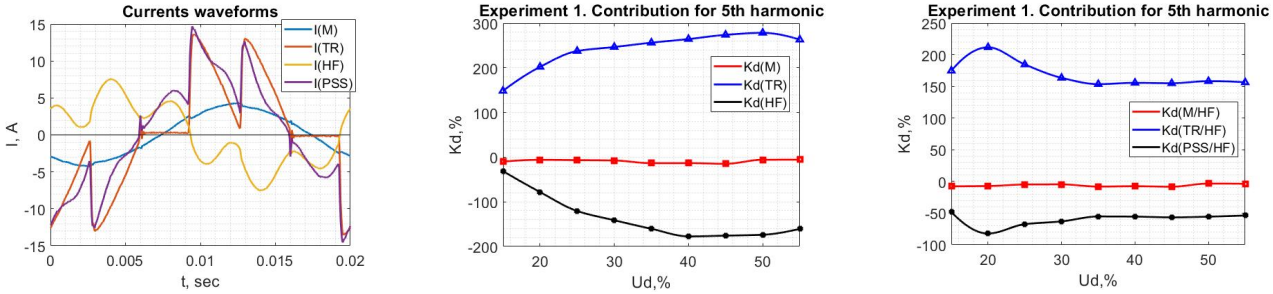

(**a**) (**b**) (**c**)

Figure 12. Results of the Experiment 1 for the 5th harmonic: (**a**) waveform of currents; (**b**) $K_D^{(h)}$ relative to the current of the PSS; (**c**) $K_D^{(h)}$ relative to the current of the filter.

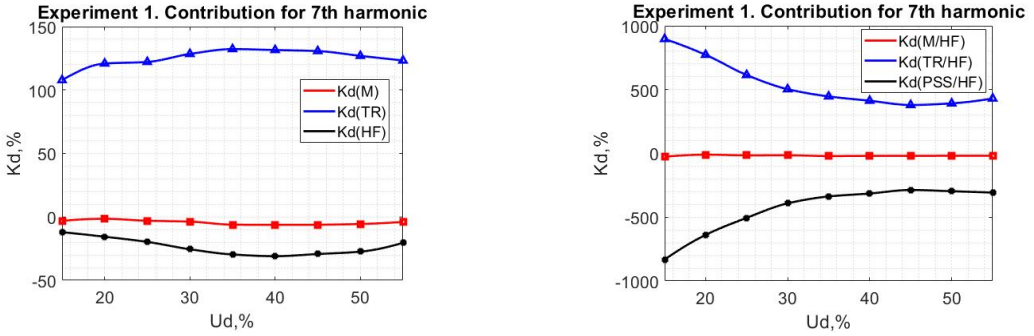

(**a**) (**b**)

Figure 13. Results of Experiment 1 for the 7th harmonic: (**a**) $K_D^{(h)}$ relative to the current of the PCC; (**b**) $K_D^{(h)}$ relative to the current of the filter.

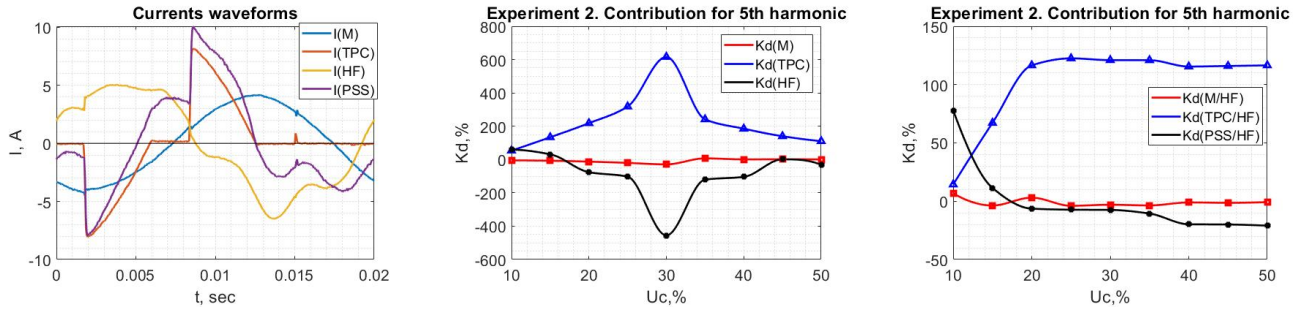

(**a**) (**b**) (**c**)

Figure 14. Results of Experiment 2 for the 5th harmonic: (**a**) waveform of currents; (**b**) $K_D^{(h)}$ relative to the current of PSS; **(c)** $K_D^{(h)}$ relative to the current of the filter.

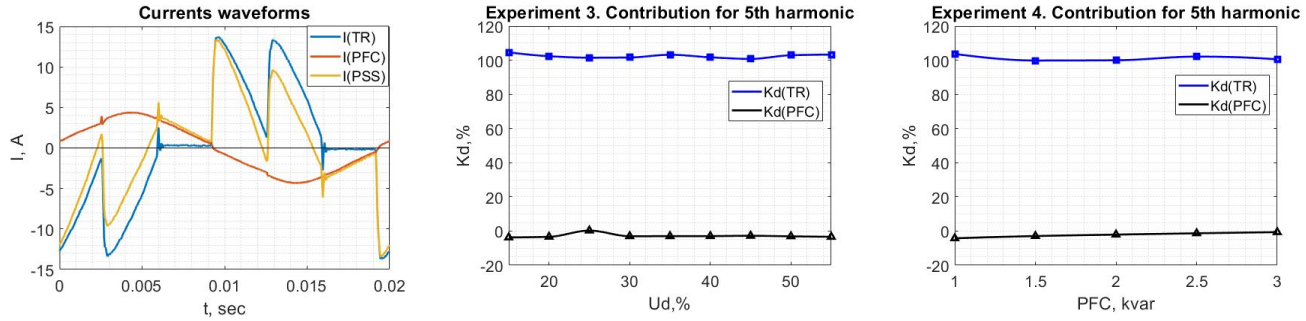

Figure 15. Results of Experiment 3 and Experiment 4 for the 5th harmonic: (**a**) waveform of currents; (**b**) $K_D^{(h)}$ relative to the current of PSS for Experiment 3; **(c)** $K_D^{(h)}$ relative to the current of PSS for Experiment 4.

It can be seen in Figure 12b that *TR's* contribution is about 265%, *M's* contribution is about −5%, and *TR's* contribution is about −160%, when U_d is more than 35%. When this value is lower, the calculation results do not give 100% in sum due to the small harmonic emissions, which do not allow an accurate calculation. It is especially notable when measurements for each consumer are not carried out simultaneously. Based on the obtained results, it can be concluded that *HF* can be characterized by a negative value of the contribution, which means *HF* compensates for the harmonic emission of other consumers whose contributions are positive. Furthermore, the contribution of *M* is still a small negative value, which shows the absence of *M's* harmonic emissions and its low compensation ability. Considering the contributions relative to $\dot{I}_{HF^{(h)}}$, in Figure 12c, it is shown that *TR* is a dominant source of harmonic currents, when current that flows through the PSS causes a negative contribution of about −55%. It indicates an absence or extremely small harmonic emission from the utility side.

Concerning the non-resonant frequency, it is shown in Figure 13a that *M's* contribution remains the same as for the 5th harmonic in Figure 12b but *HF's* contribution is about −27%, which is closer to the linear load's result. The higher the frequency, the closer the results for *M* and *HF* are. At the same time, Figure 13b presents information about the consumer's side distortion source similar to Figure 12c. However, only the results for the resonant frequency can be used for this purpose to obtain an accurate result, because the currents of the consumer and the utility flow mainly through the filter only for the resonant frequency that is shown if Figure 5b.

Similarly, Figure 14b illustrates that *TPC* is a dominant source of the 5th harmonic current. However, it can be seen that both *TPC's* and *HF's* contributions amplitudes have a maximum at U_d = 30%. This is a consequence of the fact that the amplitude of *TPC*'s 5th harmonic current has a maximum at U_d = 30%. As a result, *HF*'s 5th harmonic current has a maximum at the same point. Consequently, the current of PSS $\dot{I}_{0^{(h)}}$ decreases and leads to an increase in the contributions relative to $\dot{I}_{0^{(5)}}$ because the denominator of Formula (14) tends to zero. As in Figure 12c, Figure 14c presents information about the utility and consumer contributions and the same conclusions can be drawn in that there are no significant distortions at the utility side.

Analyzing Experiments 3 and 4 when *PFC* is connected, it can be concluded that the contribution of *PFC* is about −5% within the wide range of the nonlinear load parameters and the wide range of the *PFC's* capacitance. It means that this type of load shows results similar to *M*. In other words, it can be characterized as a linear load and cannot be mistakenly identified as a harmonic emission source.

3.2.3. Experiments of Block 3

The experiments of block 3 were conducted with additional grid side distortions created by *TPC* and resistors R_s, which is shown in Figure 16.

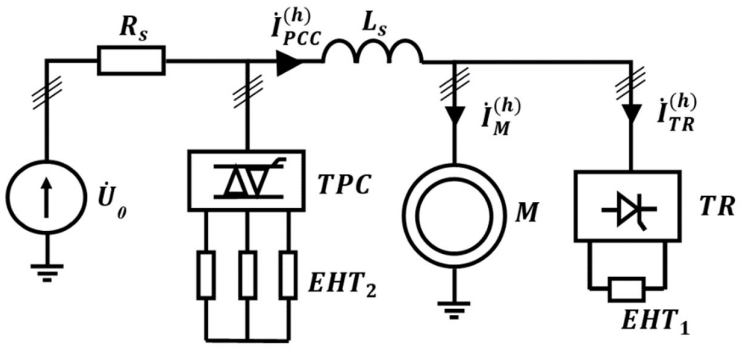

Figure 16. Laboratory branch scheme for block 3.

The parameters of the used equipment are presented in Table 3.

Table 3. The equipment parameters for the experiments of block 3.

	R_S, Ohm	*TPC* U_c%	L_S, mH	*TR*, U_d%	*M*, kW
Experiment 1	2.2	40	0.1	15÷50	1.04
Experiment 2	2.2	40	0.1	40	0÷1.04
Experiment 3	2.2	10÷50	0.1	40	1.04

Experiments 1 and 2 were similar to Experiments 1 and 2 of block 1 but with additional distortions from the grid side. Experiment 3 was carried out to evaluate the influence of external harmonic distortions on the $K_D^{(h)}$ calculation results when *M's* and *TR's* parameters were constant.

During each experiment, the harmonic currents $\dot{I}_{PCC(h)}$, $\dot{I}_{TR(h)}$, and $\dot{I}_{M(h)}$ were measured and the contributions $K_{D\,TR}^{(h)}$, $K_{DM}^{(h)}$ were calculated.

The waveforms of the currents measured during Experiments 1–3 are shown in Figure 17. The calculation of the contributions for the 5th harmonic relative to the PSS is presented in Figure 18a–c for Experiments 1–3, respectively.

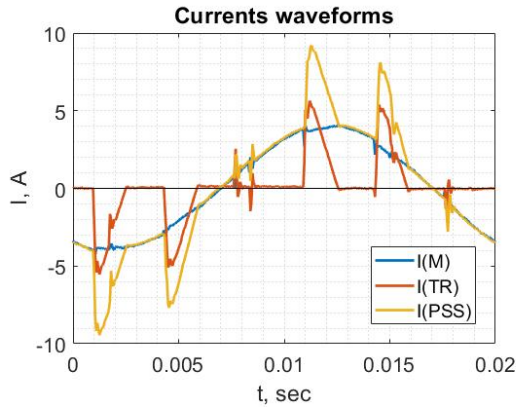

Figure 17. Waveform of the currents for the block 3 experiments.

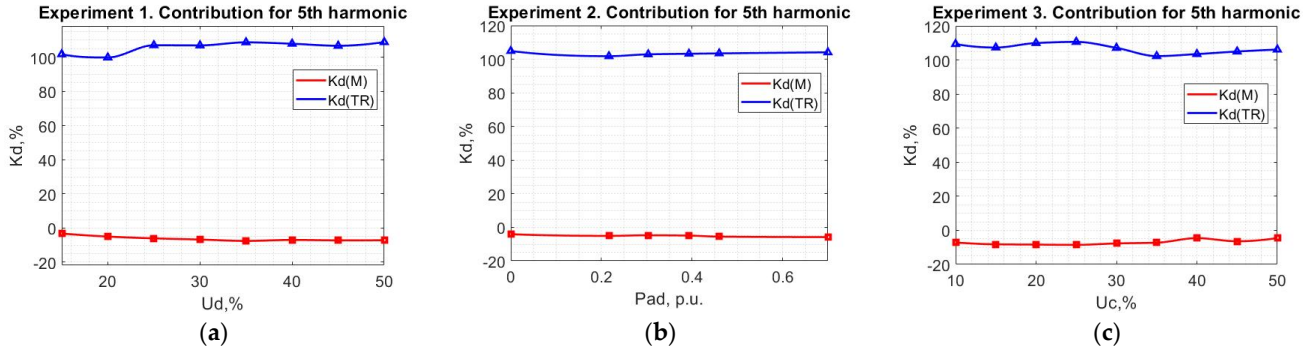

Figure 18. Results of the calculations of $K_D^{(h)}$ for the 5th harmonic: (**a**) Experiment 1; (**b**) Experiment 2; (**c**) Experiment 3.

Compared to block 1, the contribution of *TR* slightly increases from 104% to 107% and the contribution of *M* changes from −4% to −7%, which does not significantly affect the conclusions that can be drawn according to the data obtained. Concerning Experiment 3, *TPC* as a source of harmonic emission from the utility side does not significantly affect the calculation results and the changes in the $K_D^{(h)}$ values are in the confidence interval of the calculations and measurements.

3.2.4. Experiments of Block 4

The experiments of block 4 were conducted with the additional grid side distortions and capacitive loads that are shown in Figure 19.

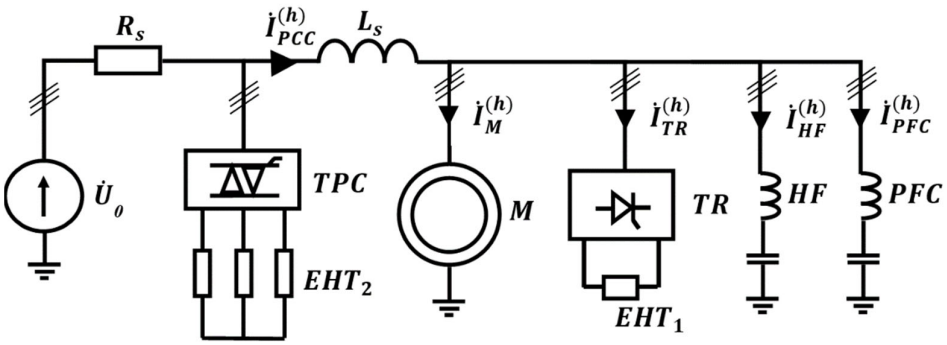

Figure 19. Laboratory branch scheme for block 4.

The parameters of the used equipment are presented in Table 4.

Table 4. The equipment parameters for the experiments of block 4.

	R_S, Ohm	*TPC*, U_d%	L_S, mH	*TR*, U_d%	*M*, kW	*HF*	*PFC's* Capacitance, kvar
Experiment 1	2.2	40	0.1	15÷55	1.04	+	-
Experiment 2	2.2	40	0.1	15÷50	1.04	-	2
Experiment 3	2.2	40	0.1	20	1.04	-	0-3
Experiment 4	2.2	10÷50	0.1	20	1.04	-	2

During each experiment, the harmonic currents $\dot{I}_{PCC}{}^{(h)}$, $\dot{I}_{TR}{}^{(h)}$, $\dot{I}_{HF}{}^{(h)}$/ $\dot{I}_{PFC}{}^{(h)}$, and $\dot{I}_{M}{}^{(h)}$ were measured and the contributions $K_{D\,TR}^{(h)}$, $K_{D\,HF}^{(h)}$/$K_{D\,PFC}^{(h)}$, and $K_{DM}^{(h)}$ were calculated relative to the current $\dot{I}_{PCC}{}^{(h)}$. In addition, the contributions $K_{D\,TR/F}^{(h)}$, $K_{D\,PCC/F}^{(h)}$, and $K_{DM/F}^{(h)}$ were found for Experiment 1. The results of the measurements and calculations for Experiment 1 when *HF* is connected at PCC are presented in Figure 20. Namely, Figure 20a shows the

waveforms of the measured currents, Figure 20b provides information about the calculated contribution relative to the current $\dot{I}_{PCC^{(h)}}$, and data about the contributions relative to the current $\dot{I}_{HF^{(h)}}$ is given in Figure 20c.

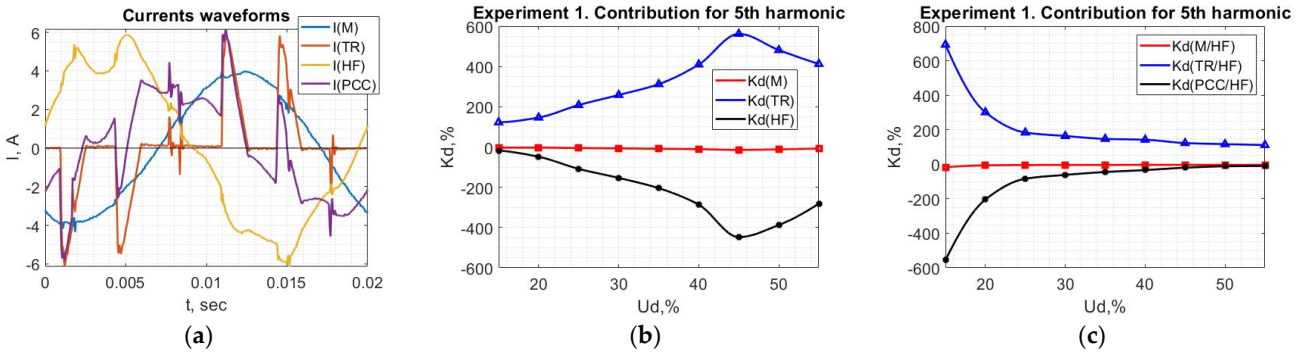

(**a**) (**b**) (**c**)

Figure 20. Results of Experiment 1 for the 5th harmonic: (**a**) waveform of currents; (**b**) $K_D^{(h)}$ relative to the current of the PCC; **(c)** $K_D^{(h)}$ relative to the current of the filter.

Similar to Experiment 1 of block 2, in Figure 20b, *TR* can be identified as the harmonic source, where current that flows through the *HF* compensates for *TR* harmonic generation, while *M* is not affected by harmonic distortions. According to Figure 20c, the created grid side emission is not enough to change the signs of the contributions of *TR* and PSS. However, in Figure 20c, it can be seen that the contribution $K_{D\,TR/HF}^{(h)}$ is smaller for $U_d >$ 30% compared to the same experiment without grid side distortion (block 2, Experiment 1, Figure 12c).

Considering Experiments 2–4, when *PFC* is connected, the oscillograms of the measured currents and voltage are provided in Figure 21a. At the same time, the contributions relative to the current of the PCC are presented in Figure 21b–d. It can be noted that *PFC's* and *M's* contribution is close to each other and these loads are clearly identified as linear. The change in the consumer's harmonic generation nor the parameters of *PFC* does not affect the calculation result. Only the varied utility side harmonic source leads to a slight decrease in the amplitudes of $K_{D\,TR}^{(h)}$ and $K_{D\,M}^{(h)}$.

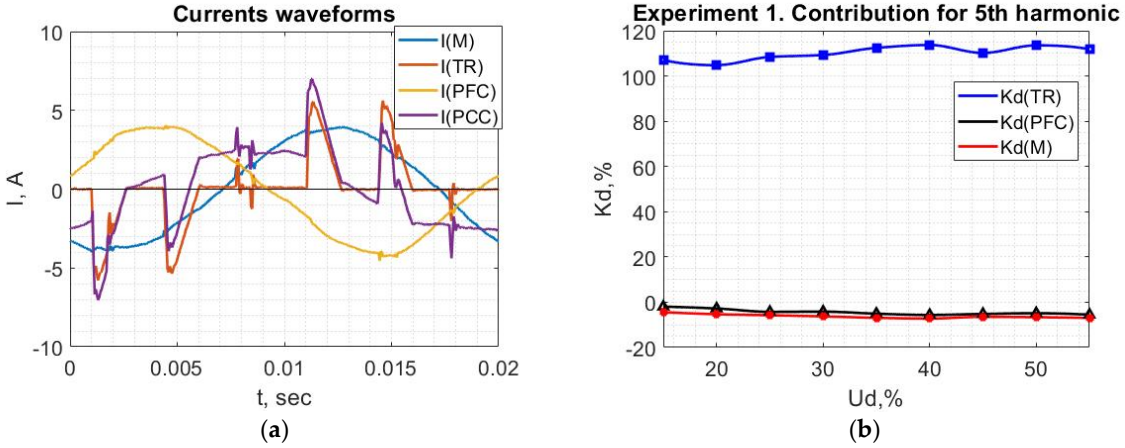

(**a**) (**b**)

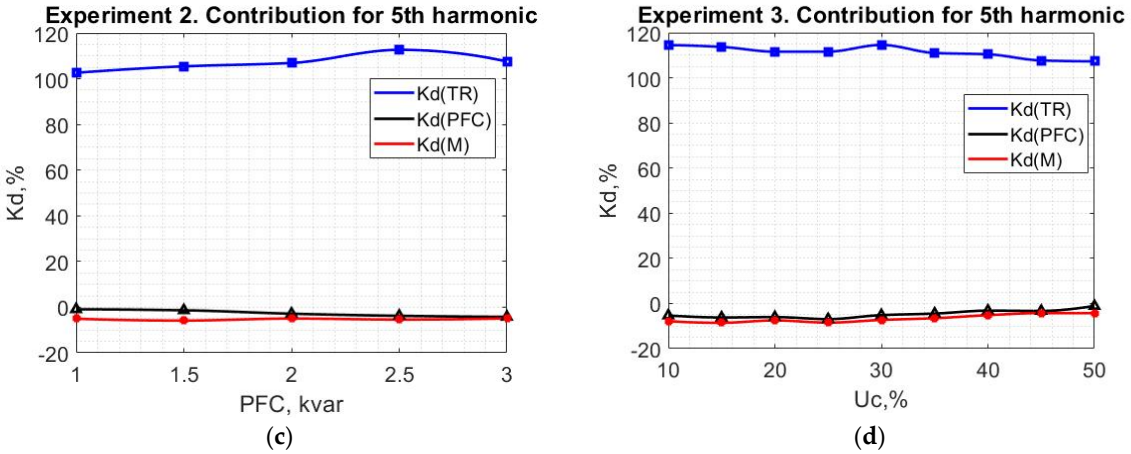

Figure 21. Results of Experiment 2–4 for the 5th harmonic: (**a**) waveform of the currents; **(b)** $K_D^{(h)}$ relative to the current of PCC for Experiment 2; **(c)** $K_D^{(h)}$ relative to the current of PCC for Experiment 3; **(d)** $K_D^{(h)}$ relative to the current of PCC for Experiment 4.

4. Discussions

Based on the algorithm proposed in Section 2.3, we can analyze the results obtained during the laboratory experiments.

Concerning the identification of the utility contribution to the distortion of current and voltage at the PCC, Experiment 1 of block 2 and Experiment 1 of block 4 should be considered. It can be seen that the calculated contributions $K_{D\,TR/HF}^{(h)}$ and $K_{D\,0/HF}^{(h)}$ clearly identify that *TR* is a source of harmonic currents when there is a small amount of harmonic emission from the utility side. At the same time, when a grid side distortion appears, as shown in block 4, the contribution $K_{D\,TR/HF}^{(h)}$ decreases from 156% to 125% and the contribution $K_{D\,0/HF}^{(h)}$ rises from −55% to −23% compared to block 2. This result illustrates how external distortion affects the calculations of the contributions relative to the filter's current and confirms that this approach is applicable for these conditions. Based on the obtained values of the contribution, it is possible to conclude whether the utility is responsible for harmonic distortion at PCC. If $K_{D\,0/HF}^{(h)}$ is more than 50%, any compensation measured from the consumer side do not reach the expected result. Thus, one of the tasks of further research is to create conditions that allow $K_{D\,0/HF}^{(h)} > 50\%$ to be obtained in order to confirm this thesis experimentally.

In the case when the utility is not a dominant source of distortions, it is possible to move to the next step of the algorithm and share the responsibilities for harmonic generation between consumers or parts of the consumer's energy system. Analyzing the rest of the experiments, the following conclusions can be drawn:

- Regardless of the external conditions, the contribution of the linear load like *M* is negative and has a small amplitude compared to other consumers;
- Nonlinear loads have positive contributions that may exceed 100% and directly depend on the harmonic currents generated by these loads compared with the PSS harmonic current in vector form;
- Harmonic filters for a resonant frequency have negative contributions, the amplitudes of which are rather higher than linear loads' amplitudes. This clearly indicates that currents that flow through the filter compensates for nonlinear loads' harmonic emissions;
- Harmonic filters for non-resonant frequencies as well as power factor correctors with a detuned frequency show the properties of linear loads and their contributions are negative and have a low amplitude; however, power factor correctors without a detuned frequency should be considered separately.

5. Conclusions

The following results were found from this study:

- Two indices were introduced to evaluate the grid side distortions and share the responsibilities for harmonic current emission between consumers;
- Based on the proposed indices, the method's algorithm was completed, which allows identification of harmonic sources and evaluation of their influence on the current distortion at the PCC;
- The experiments' results have shown that this method clearly identifies harmonic emissions as a percentage correlation and cannot mistakenly classify a capacitive load as a source of distortion.

Obviously, additional research is required on:

- Significant grid side emission ($K_{D\,0/HF}^{(h)} > 50\%$);
- A wider range of linear load types;
- A wider range of nonlinear load types;
- Power factor correctors without a detuned frequency.

To sum up, it can already be concluded that the proposed indices K_D and $K_{D/F}$ can be used as a tool to quantify the responsibility for harmonic current generation between the utility and consumers.

Author Contributions: Conceptualization, Y.S.; Data curation, A.S.; Formal analysis, I.D.; Investigation, I.D.; Methodology, I.D.; Resources, V.D. and A.S.; Software, V.D.; Supervision, M.J.C.; Writing—original draft, I.D.; Writing—review and editing, Y.S. and M.J.C. All authors have read and agreed to the published version of the manuscript.

Funding: The reported study was funded by RFBR, project number 20-38-90096.

Institutional Review Board Statement: Not applicable.

Informed Consent Statement: Not applicable.

Conflicts of Interest: The authors declare no conflict of interest.

References

1. Ahmad, Z.; Torres, J.R.; Kumar, N.V.; Rakhshani, E.; Palensky, P.; van der Meijden, M. A Power Hardware-in-the-Loop Based Method for FAPR Compliance Testing of the Wind Turbine Converters Control. *Energies* **2020**, *13*, 5203, doi:10.3390/en13195203.
2. Janardhan, K.; Mittal, A.; Ojha, A. Performance investigation of stand-alone solar photovoltaic system with single phase micro multilevel inverter. *Energy Rep.* **2020**, *6*, 2044–2055, doi:10.1016/j.egyr.2020.07.006.
3. Vasilyev, B.Y.; Shpenst, V.A.; Kalashnikov, O.V.; Ulyanov, G.N. Providing energy decoupling of electric drive and electric grids for industrial electrical installations. *J. Min. Inst.* **2018**, *229*, 41–49, doi:10.25515/PMI.2018.1.41.
4. Zhen, Q.; Di, Q. Soft-switching technology of three-phase six-switch PFC rectifier. *Energies* **2020**, *13*, 1–15, doi:10.3390/en13195130.
5. Kozyaruk, A.E.; Kamyshyan, A.M. Improving the energy efficiency of the electromechanical transmission of an open-pit dump truck. *J. Min. Inst.* **2019**, *239*, 576–582, doi:10.31897/PMI.2019.5.576.
6. Zamyatin, E.; Voytyuk, I.; Zamyatina, E. Increasing the energy efficiency of an enterprise by point compensating of power quality distortions. *E3S Web Conf.* **2019**, *140*, 1–6, doi:10.1051/e3sconf/201914004010.
7. Munoz-Guijosa, J.M.; Kryltcov, S.B.; Solovev, S.V. Application of an active rectifier used to mitigate currents distortion in 6-10 KV distribution grids. *J. Min. Inst.* **2019**, *236*, 229–238, doi:10.31897/PMI.2019.2.229.
8. Belsky, A.A.; Yu Glukhanich, D.; Ivanchenko, D.I. Remote area power supply system for oil leakage detection systems and stop valves drives for pipelines. *J. Phys. Conf. Ser.* **2020**, *1652*, 012032, doi:10.1088/1742-6596/1652/1/012032.
9. Diahovchenko, I.; Volokhin, V.; Kurochkina, V.; Špes, M.; Kosterec, M. Effect of harmonic distortion on electric energy meters of different metrological principles. *Front. Energy* **2019**, *13*, 377–385, doi:10.1007/s11708-018-0571-1.
10. Janik, P.; Kosobudzki, G.; Schwarz, H. Influence of increasing numbers of RE-inverters on the power quality in the distribution grids: A PQ case study of a representative wind turbine and photovoltaic system. *Front. Energy* **2017**, *11*, 155–167, doi:10.1007/s11708-017-0469-3.
11. Skamyin, A.N.; Kovalchuk, M.S. Energy Efficiency Improving of Reactive Power Compensation Devices. In Proceedings of the Conference of Russian Young Reseachers in Electrical and Electronic Engineering, St. Petersburg, Russia, 29 January–1 February 2018; pp.780–783, doi:10.1109/EIConRus.2018.8317207.

12. Bardanov, A.I.; Pudkova, T. V. Application of Power Theory for Electricity Metering in Presence of Distortion. In *IOP Conference Series: Materials Science and Engineering*; IOP Publishing: Bristol, UK, 2019; Volume 643, doi:10.1088/1757-899X/643/1/012011.
13. Rastvorova, I.I. Assessment of the Consumers' Contribution to the Deterioration of the Electrical Power Quality.In *IOP Conference Series: Materials Science and Engineering;* IOP Publishing: Bristol, UK, 2019; Volume 643, doi:10.1088/1757-899X/643/1/012010.
14. Benaissa, A.; Rabhi, B.; Moussi, A. Power quality improvement using fuzzy logic controller for five-level shunt active power filter under distorted voltage conditions. *Front. Energy* **2014**, *8*, 212–220, doi:10.1007/s11708-013-0284-4.
15. Jin, T.; Chen, Y.; Guo, J.; Wang, M.; Mohamed, M.A. An effective compensation control strategy for power quality enhancement of unified power quality conditioner. *Energy Reports* **2020**, *6*, 2167–2179, doi:10.1016/j.egyr.2020.07.027.
16. Kularbphettong, K.; Boonseng, C. HPFs filtering solutions for reduced the harmonic current generated by SMPS and ac drive systems. *Energy Reports* **2020**, *6*, 648–658, doi:10.1016/j.egyr.2019.11.133.
17. Lv, Z.; Sun, L.; Duan, J.; Duan, M.; Pei, H. A novel harmonic impedance compensator based on POHMR-type RC under gird voltage distortion. *Int. J. Electr. Power Energy Syst.* **2021**, *124*, 106352, doi:10.1016/j.ijepes.2020.106352.
18. Saim, A.; Houari, A.; Ait-Ahmed, M.; Machmoum, M.; Guerrero, J.M. Active resonance damping and harmonics compensation in distributed generation based islanded microgrids. *Electr. Power Syst. Res.* **2021**, *191*, 106900, doi:10.1016/j.epsr.2020.106900.
19. Salman, M.; Haq, I.U.; Ahmad, T.; Ali, H.; Qamar, A.; Basit, A.; Khan, M.; Iqbal, J. Minimization of total harmonic distortions of cascaded H-bridge multilevel inverter by utilizing bio inspired AI algorithm. *Eurasip J. Wirel. Commun. Netw.* **2020**, *2020*, 1–12, doi:10.1186/s13638-020-01686-5.
20. Sychev, Y.A.; Abramovich, B.N.; Zimin, R.Y. Modelling and analysis of functional modes of active compensators in distributed generation systems. *J. Phys. Conf. Ser.* **2019**, *1333*, 062028, doi:10.1088/1742-6596/1333/6/062028.
21. Akagi, H. A New Method of Harmonic Power Detection Based on the Instantaneous Active Power in Three-Phase Circuits. *IEEE Trans. Power Deliv.* **1995**, *10*, 1737–1742, doi:10.1109/61.473386.
22. Swart, P.H.; Case, M.J.; Van Wyk, J.D. On techniques for localization of sources producing distortion in electric power networks. *Eur. Trans. Electr. Power* **1994**, *4*, 485–489, doi:10.1002/etep.4450040611.
23. Xu, W.; Liu, Y. A method for determining customer and utility harmonic contributions at the point of common coupling. *IEEE Trans. Power Deliv.* **2000**, *15*, 804–811, doi:10.1109/61.853023.
24. Barbaro, P.V.; Cataliotti, A.; Cosentino, V.; Nuccio, S. A novel approach based on nonactive power for the identification of disturbing loads in power systems. *IEEE Trans. Power Deliv.* **2007**, *22*, 1782–1789, doi:10.1109/TPWRD.2007.899624.
25. Stevanović, D.; Petković, P. A single-point method based on distortion power for the detection of harmonic sources in a power system. *Metrol. Meas. Syst.* **2014**, *21*, 3–14, doi:10.2478/mms-2014-0001.
26. Xu, W. Power direction method cannot be used for harmonic source detection. *Proc. IEEE Power Eng. Soc. Transm. Distrib. Conf.* **2000**, *2*, 873–876, doi:10.1109/pess.2000.867472.
27. Safargholi, F.; Malekian, K.; Schufft, W. On the Dominant Harmonic Source Identification-Part II: Application and Interpretation of Methods. *IEEE Trans. Power Deliv.* **2018**, *33*, 1278–1287, doi:10.1109/TPWRD.2017.2751673.
28. Davis, E.J.; Emanuel, A.E.; Pileggi, D.J. Harmonic pollution metering: Theoretical considerations. *IEEE Trans. Power Deliv.* **2000**, *15*, 19–23, doi:10.1109/61.847223.
29. Fernandez, F.M.; Chandramohanan Nair, P.S. Method for separation of customer and utility contributions of harmonics at point of common coupling. *IET Gener. Transm. Distrib.* **2013**, *7*, 374–381, doi:10.1049/iet-gtd.2012.0361.
30. Castaldo, D.; Fenvro, A.; Salicone, S.; Testa, A. A power-quality index based on multi-point measurements. **2004**, *4*, 722–726, doi:10.1109/ptc.2003.1304806.
31. Santos, A.C.; Oliveira, J.C.; Santos, I.N. A comparative analysis between methodologies for responsibility assignment on harmonic distortions. *Renew. Energy Power Qual. J.* **2015**, *1*, 305–310, doi:10.24084/repqj13.312.
32. Srinivasan, K.; Jutras, R. Conforming and non-conforming current for attributing steady state power quality problems. *IEEE Trans. Power Deliv.* **1998**, *13*, 212–217, doi:10.1109/61.660880.
33. Pavas, A.; Staudt, V.; Torres-Sánchez, H. Experimental Investigation of Existing Methodologies for the Responsibilities Assignment Problem. In Proceedings of the 2009 IEEE Bucharest PowerTech Innovation Ideas Towards the Electrical Grid of the Future, Bucharest, Romania, 28 June–2 July 2009; doi:10.1109/PTC.2009.5281856.
34. Xu, W.; Li, C.; Tayjasanant, T. A "critical impedance" based method for identifying harmonic sources. **2005**, *19*, 917–917, doi:10.1109/pes.2004.1372959.
35. Shklyarskiy, Y.; Skamyin, A.; Vladimirov, I.; Gazizov, F. Distortion load identification based on the application of compensating devices. *Energies* **2020**, *13*, 1–13, doi:10.3390/en13061430.